THE UNIVERSITY of EDINBURGH

Edinburgh Research Explorer

Laser-induced nucleation of carbon dioxide bubbles

Citation for published version:
Ward, MR, Jamieson, W, Leckey, C & Alexander, A 2015, 'Laser-induced nucleation of carbon dioxide bubbles', *The Journal of Chemical Physics*, vol. 142, no. 144501, 144501.
https://doi.org/10.1063/1.4917022

Digital Object Identifier (DOI):
10.1063/1.4917022

Link:
Link to publication record in Edinburgh Research Explorer

Document Version:
Publisher's PDF, also known as Version of record

Published In:
The Journal of Chemical Physics

Publisher Rights Statement:
(c) 2015 AIP Publishing LLC

General rights
Copyright for the publications made accessible via the Edinburgh Research Explorer is retained by the author(s) and / or other copyright owners and it is a condition of accessing these publications that users recognise and abide by the legal requirements associated with these rights.

Take down policy
The University of Edinburgh has made every reasonable effort to ensure that Edinburgh Research Explorer content complies with UK legislation. If you believe that the public display of this file breaches copyright please contact openaccess@ed.ac.uk providing details, and we will remove access to the work immediately and investigate your claim.

Download date: 04. May. 2024

Laser-induced nucleation of carbon dioxide bubbles

Martin R. Ward, William J. Jamieson, Claire A. Leckey, and Andrew J. Alexander[a)]
School of Chemistry, University of Edinburgh, Edinburgh EH9 3JJ, Scotland

(Received 28 February 2015; accepted 26 March 2015; published online 8 April 2015)

A detailed experimental study of laser-induced nucleation (LIN) of carbon dioxide (CO_2) gas bubbles is presented. Water and aqueous sucrose solutions supersaturated with CO_2 were exposed to single nanosecond pulses (5 ns, 532 nm, 2.4–14.5 MW cm^{-2}) and femtosecond pulses (110 fs, 800 nm, 0.028–11 GW cm^{-2}) of laser light. No bubbles were observed with the femtosecond pulses, even at high peak power densities (11 GW cm^{-2}). For the nanosecond pulses, the number of bubbles produced per pulse showed a quadratic dependence on laser power, with a distinct power threshold below which no bubbles were observed. The number of bubbles observed increases linearly with sucrose concentration. It was found that filtering of solutions reduces the number of bubbles significantly. Although the femtosecond pulses have higher peak power densities than the nanosecond pulses, they have lower energy densities per pulse. A simple model for LIN of CO_2 is presented, based on heating of nanoparticles to produce vapor bubbles that must expand to reach a critical bubble radius to continue growth. The results suggest that non-photochemical laser-induced nucleation of crystals could also be caused by heating of nanoparticles. © *2015 AIP Publishing LLC.* [http://dx.doi.org/10.1063/1.4917022]

I. INTRODUCTION

Gas nucleation is a process of great significance in science. The process is important in oil and natural gas recovery, power and steam generation, electrolysis, polymer production, and waste treatment.[1] Bubbles are an essential feature in numerous beverages and foods. Gas nucleation poses a dangerous phenomenon to divers, who can suffer from decompression sickness or the so-called "bends," named after the "Grecian bend" posture adopted by victims. Cavitation, the formation of vapor cavities in liquids at extremes of shear or pressure, is also a gas nucleation process and can cause damage to pumps and propellers.[2] As with most nucleation processes, the study of gas nucleation dynamics is hindered by its stochastic nature; remote control of the location and time of bubble nucleation would significantly broaden opportunities for experimental research.

Non-photochemical laser-induced nucleation (NPLIN) was introduced by Garetz and co-workers as a new phenomenon in the context of crystal nucleation.[3] It was found that pulses of laser light of nanosecond duration would cause formation of crystals in metastable supersaturated solutions of urea. The phenomenon was termed "non-photochemical" on the basis that the low power and long wavelength of the light used, in conjunction with apparently no accessible electronic states of the solute or the solvent, meant that a photochemical mechanism was ruled out. Additional evidence, including alignment of initial crystallites along the electric field[3] and control of crystal structure of glycine through polarization of the light,[4] suggests that the electric field has a directional influence on the solute. NPLIN has been observed for a range of solutes including inorganic salts, small organic molecules, pure liquids, and proteins.[5] The mechanism for NPLIN is thought to rely on formation of pre-nucleating clusters of solute that become stabilized in the strong, transient electric field of a pulse of laser light.[3,6,7] In the case of small organic molecules, a Kerr effect at optical frequencies is thought to align clustered molecules relative to the electric field.[8] However, calculations indicate that the energy of alignment of an induced dipole is only $\sim 10^{-4}\ k_B T$, i.e., random thermal fluctuations will destroy the alignment.[9] It has been suggested that co-operative effects from multiple molecules in pre-nucleating clusters could explain the deficit, but model simulations suggest otherwise.[10]

LIN of carbon dioxide (CO_2) bubbles from carbonated water by pulsed laser light has been observed by Knott *et al.*[11] They showed that the threshold laser pulse energy decreased with increasing supersaturation of CO_2. The nanosecond durations and pulse energies of the laser light were commensurate with those used for NPLIN of crystals. It has been pointed out that the mechanisms used to explain nucleation of solids are not appropriate for gases, since the prototypical cluster is surely less dense, and co-operative effects are therefore ruled out.[10] Knott *et al.* also showed that rapid shaking of solutions supersaturated with both glycine and argon induced formation of glycine crystals. The authors suggested that cavitation by small (possibly nanoscale) bubbles could explain both LIN of CO_2 and NPLIN of crystals. It should be noted that NPLIN experiments are distinct from experiments where cavitation is induced deliberately to cause crystallization, e.g., by focusing an intense beam of light.[12,13]

To build on the exploratory work of Knott *et al.*, we have conducted a detailed study of LIN in carbonated sugar solutions. We present measurements of the dependence of bubble count on laser power and we pay particular attention to filtering of solutions. We develop a simple model to describe our results in terms of transient heating of nanoparticles. The results

a)e-mail: andrew.alexander@ed.ac.uk

 © 2015 AIP Publishing LLC

suggest that there is a population of nanoparticles weighted towards smaller particle size. We conclude our discussion with an evaluation of viable mechanisms for NPLIN of crystals, based on the evidence so far.

II. METHODS

All of the glasswares used for the experiments were washed thoroughly using warm soapy water and rinsed several times with filtered water. Ultrapure water was obtained from a water purification system (resistivity 18.2 MΩ cm, Sartorius arium 611 UV). Disposable filters (polyethersulfone membrane, 0.22 μm, Millex GP) were used at several stages to remove and avoid ingress of solid impurity particles. Sucrose (Sigma–Aldrich, ≥99.5%) was used as received. Sucrose solutions were prepared at concentrations of 2, 4, 6, 8, and 16 g per 100 g of water (corresponding to molalities of 0.058, 0.11, 0.18, 0.23, and 0.47 mol kg^{-1}). For comparison, a typical sugary soda drink contains ∼11 g sugar per 100 cm^3. Sucrose solutions were used either as prepared or filtered through a 0.22 μm filter. Approximately 150 cm^3 of solution was transferred to a borosilicate glass bottle with the screw-cap modified to include stainless-steel tube fittings (Swagelok Cajon Ultra-Torr). Septa were secured inside the fittings to allow gas transfer through a hypodermic needle (23 gauge).

Samples were supersaturated with CO_2 gas as follows. The samples were chilled in a fridge at 6 °C for one hour, since CO_2 has a greater solubility at lower temperatures. Samples were removed from the fridge and over-pressurized with CO_2 gas (BOC Industrial Gases, U.K., 99.8%, passed through a 0.22 μm filter) to a total pressure of 270 kPa (170 kPa over atmospheric pressure). Bottles were shaken twenty times to promote dissolution. The headspace of the bottle was re-pressurized with CO_2 at 170 kPa before being returned to the fridge for 2 h. The carbonation process was repeated twice more. After the final 2 h in the fridge, any remaining pressure present in the headspace of the bottle was released gently. Sample solutions were left in the fridge until ready to be nucleated by the laser. The supersaturation (S) of CO_2 was calculated as $S = C/C_{sat}$, where C_{sat} is the saturation concentration of gas (mol. CO_2/mol. water). Efficacy of the carbonation procedure was verified by a simple titrimetric method based on that of Crossno *et al.*[14] The carbonation procedure was found to be reliably reproduced, with no significant differences observed between CO_2 dissolution for filtered or unfiltered solutions at 3 different sucrose concentrations.

Prior to shooting with the laser, solutions were transferred gently into a champagne flute and allowed to warm to ambient temperature (20 °C). Solutions were shot with single laser pulses from a Nd^{3+}:YAG laser (Continuum, Surelite II-10, 532 nm wavelength, 5 ns pulse duration). Prior to intersection with the flute, the laser beam was passed through an iris (5.5 mm) and a Glan-laser polarizer which was angle-tuned to control the power of the linearly polarized beam. The mean power (in W) of the beam was measured using a power meter (Nova, Ophir) with the laser operating at 10 Hz. The curvature of the flute causes a slight focusing of the beam within the solution, which was accounted for by using a simple ray-tracing procedure. The peak power density (j_{peak}) was calculated as the average of the power density values at the front and back faces of the flute. For water at 20 °C with refractive index n_w = 1.3354,[15] we calculate 0.1 W (10 mJ pulse^{-1}) corresponds to energy density u = 630 J m^{-2} and peak power density j_{peak} = 12 MW cm^{-2}. Refractive indices for sucrose solutions were obtained by interpolation of tabulated data.[16]

At each laser power, the sample was shot 5 times, with 20 s delay between each of the pulses. The nucleation procedure was filmed using a digital camera placed behind an orange glass filter (OG570, Schott glass) to block out the laser light, and the bubbles produced with each pulse were counted from frames of the video.

Special filtering and cleaning was used to study the effects of impurities. The special filters used were disposable syringe filters (Whatman Anotop 25, 0.02 μm). Vials were optionally cleaned by soaking in concentrated nitric acid or 10% formic acid solution for several hours before rinsing with filtered ultrapure water.

To test the effect of pulse duration on LIN, unfiltered samples of tap water and sucrose (0.48 mol kg^{-1}) in ultrapure water were carbonated by the same method described above and were exposed to femtosecond pulses from a Ti:sapphire laser (Coherent Legend Elite regenerative amplifier, 800 nm wavelength, 110 fs duration, 5.5 mm diameter beam). Mean pulse powers (1 kHz repetition rate) of 0.52 and 210 mW were used, equivalent to peak power densities in the sample of 28 MW cm^{-2} and 11 GW cm^{-2}, or energy densities per pulse of 3.3 and 13 J m^{-2}, respectively. It should be noted that although the peak power densities are higher, the energy densities of the femtosecond laser pulses are lower than the nanosecond laser pulses. Samples were exposed to either single pulses or trains of pulses at 1 kHz repetition rate.

III. RESULTS

A photograph illustrating the nucleation of bubbles caused by the passage of a laser pulse is shown in Fig. 1. After

FIG. 1. Photograph of nucleation of carbon dioxide bubbles caused by passage of the laser pulse (5 ns pulse duration) from left to right. For illustration purposes, a high laser power (∼60 MW cm^{-2}) was used to create many bubbles.

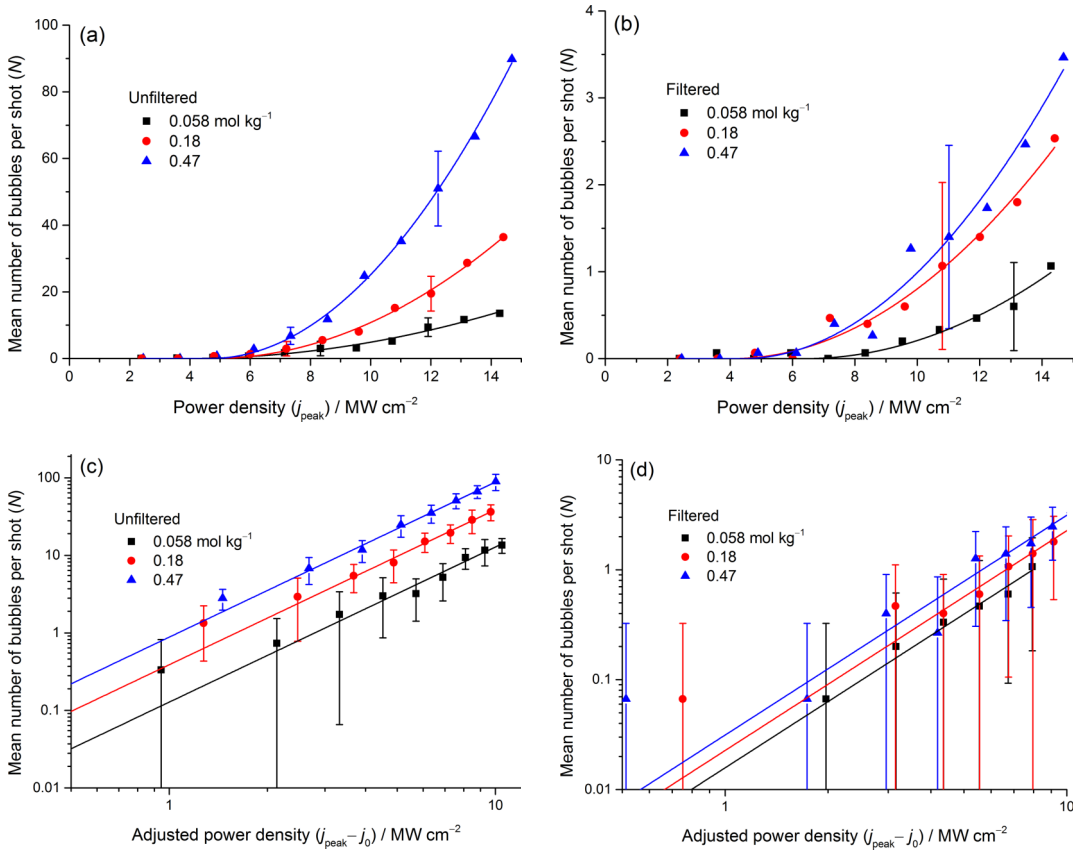

FIG. 2. Mean number of bubbles counted versus laser power density for samples with different sucrose concentrations: (a) unfiltered solutions and (b) filtered solutions. Laser pulse duration was 5 ns. Solid points are experimental results and lines represent fits obtained with a quadratic function (see text for details). Log–log plots of the same data are shown in (c) and (d), where the power values have been adjusted by subtracting the fitted threshold in each case. Sucrose concentrations are given in the legends; for clarity, only results for three concentrations have been plotted. Error bars were calculated as single standard deviations from 5 shots. The results show a threshold power density and a quadratic increase in number of bubbles nucleated as a function of laser power. The number of bubbles produced in unfiltered solutions is substantially higher than in filtered solutions.

nucleation, the bubbles were observed to accelerate vertically upwards due to growth and increase in buoyancy. We observed that each pulse produced a range of bubble sizes, suggesting that bubbles nucleate and grow under slightly different conditions. In Fig. 2 we show that the number of bubbles nucleated increases non-linearly with laser power density. Many more bubbles were observed for the unfiltered solutions compared to filtered solutions, and the number of bubbles increases with sucrose concentration. A threshold power density, below which no bubbles were nucleated, is also apparent. Similar threshold powers have been observed previously for NPLIN of crystals.[6,9,17]

The experimental data were modeled using the following expressions:

$$\begin{aligned} N &= m\,(j_{\text{peak}} - j_0)^2, \quad (j_{\text{peak}} \geq j_0), \\ N &= 0, \quad (j_{\text{peak}} < j_0), \end{aligned} \tag{1}$$

where N is the number of bubbles, j_{peak} is the power density, j_0 is the threshold power density, and m is the lability. The lability is a measure of how susceptible the sample is to LIN; higher lability means more nucleation events at a given power density. A nonlinear least-squares method was used to fit the data. In preliminary fitting of the unfiltered data, we found that the exponent in Eq. (1) was very close to 2 (i.e., quadratic) for all concentrations; therefore, we fixed it to be exactly 2 for all subsequent fits. The fit parameters for each sample are given in Table I. The filtered samples show more variability in the threshold and lability parameters, and this is due to the much lower bubble counts. It appears that filtering removes most of the cause of the nucleation, making the results more susceptible to systematic variability in cleaning and filtering, as we shall discuss further below.

The weighted mean thresholds were calculated to be 4.6 ± 0.1 MW cm^{-2} (unfiltered) and 4.8 ± 0.3 MW cm^{-2} (filtered). These threshold values are very similar to those observed from NPLIN of crystals from solution; Ward and Alexander measured thresholds of 4.8 ± 0.3 MW cm^{-2} and 5.6 ± 0.5 MW cm^{-2} for KBr and KCl solutions at 532 nm, respectively.[17] The similarity of the thresholds suggests that the mechanism for NPLIN of crystals is closely linked to that of bubbles. However, the quadratic dependence of the number of bubbles versus power density is different in comparison to the linear dependence observed for NPLIN of crystals.[6] We shall discuss this link in more detail in Sec. IV F.

Plots of lability versus sucrose concentration are shown in Fig. 3. The dependence is approximately linear for both filtered and unfiltered samples. The results shown in Figs. 2 and 3 suggest that nucleation occurs as a result of species that can be removed by filtration, and that these species are introduced

TABLE I. Threshold powers and labilities obtained by fitting the experimental data (Fig. 2) using the model function, Eq. (1). Standard errors from the nonlinear least-squares fitting procedure are also given.

Sucrose concentration/mol kg^{-1}	Threshold power density (j_0)/MW cm^{-2}	Lability (m)/cm^4 MW^{-2}
	Unfiltered samples	
0.058	3.8 ± 0.5	0.13 ± 0.02
0.12	4.3 ± 0.5	0.31 ± 0.04
0.18	4.7 ± 0.2	0.39 ± 0.02
0.23	4.7 ± 0.3	0.69 ± 0.05
0.47	4.7 ± 0.1	0.88 ± 0.03
	Filtered samples	
0.058	6.4 ± 0.6	0.016 ± 0.003
0.12	0.9 ± 1.5	0.015 ± 0.004
0.18	4.1 ± 0.5	0.023 ± 0.003
0.23	5.4 ± 0.7	0.038 ± 0.007
0.47	4.4 ± 0.6	0.031 ± 0.005

by the sucrose solute. The origin and nature of these species are not certain. They may be *extrinsic*, e.g., impurity particles in the sucrose or they may be *intrinsic*, e.g., solute clusters that grow in solution.

To test the hypothesis that impurity particles may be responsible for LIN of bubbles, we compared filtered and unfiltered samples of carbonated water, including tap water and ultrapure water from the purifier. In addition, two special samples were prepared by soaking glassware in either nitric acid or formic acid, followed by rinsing and filling with ultrapure water passed through filters with narrower pores (20 nm) than our standard filters. The measured data were fitted using the quadratic function of Eq. (1), and the results are summarized in Fig. 4. It can be seen that the thresholds for all of the filtered samples are very similar, lying in the range 4.3–4.8 MW cm^{-2}; thresholds for unfiltered samples are generally lower.

There is a clear trend of decreasing lability with better filtering and cleaning. The lability for the nitric acid results

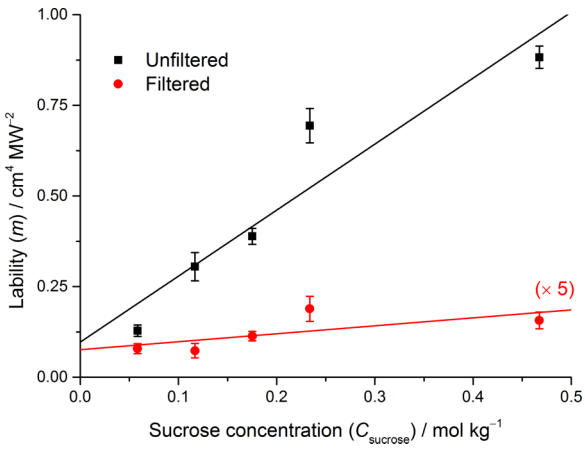

FIG. 3. Graph of lability versus sucrose concentration for unfiltered (squares) and filtered (circles) samples. Solid lines represent linear fits to the data. Data for the filtered samples have been multiplied by a factor of 5 in order to plot them on the same scale as data for the unfiltered samples.

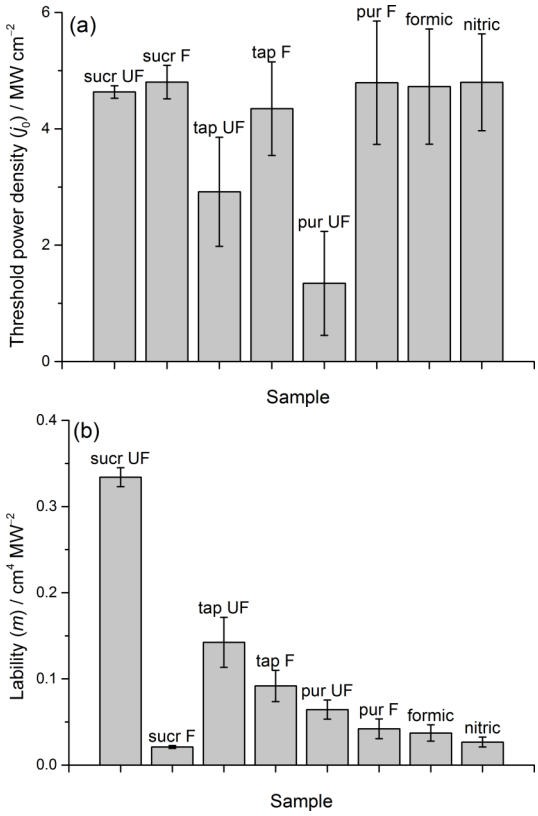

FIG. 4. Column graphs showing (a) threshold power densities and (b) labilities for samples that have undergone different treatments prior to carbonation. Key: unfiltered (UF) or filtered (F) with 0.22-μm pore filters; tap water (tap); ultrapure water from purifier (pur); sucrose solution (sucr) made with ultrapure water; glassware pre-soaked with formic acid (formic) or nitric acid (nitric), then rinsed and filled with water using 20-nm pore filters. The columns for the sucrose solution results represent the weighted means of the data given in Table I.

corresponds to ~2 bubbles per laser pulse at the highest power densities (14.2 MW cm^{-2}). Although the filtering and cleaning procedures reduce the number of bubbles, these procedures are not sufficient to stop the effect; we believe that this is due to the difficulty in preparing perfectly clean samples of water under normal laboratory conditions. The results of Fig. 4 support the hypothesis that extrinsic particles are one of the causes of LIN of bubbles. In the case of sucrose solutions, however, the solute evidently brings additional particles; we cannot say whether these additional particles are extrinsic (e.g., impurities) or intrinsic (e.g., solute clusters).

Remarkably, unfiltered samples of carbonated tap water and 0.47 mol kg^{-1} sucrose solutions that were exposed to single, femtosecond pulses (110 fs) at 28 MW cm^{-2} or 11 GW cm^{-2} did not produce any bubbles. The same samples were soon after exposed to nanosecond (5 ns) pulses at 24 MW cm^{-2} and numerous bubbles were observed, as expected from the results described above. These results suggest that the mechanism for LIN of CO_2 is non-photochemical, since the high power densities of the femtosecond pulses would be expected to favor non-linear, multiphoton ionization processes. When exposed to a train of fs pulses at 1 kHz repetition rate, occasional bubbles were observed, which may indicate occurrence of rare photochemical events requiring multiple pulses. We have previously noted that fs pulses do not induce

nucleation in NPLIN of KCl samples,[18] supporting the hypothesis that the mechanism of LIN of CO_2 and NPLIN of crystals has a common origin.

IV. DISCUSSION

A. Metastability of carbonated solutions

We begin by considering the metastability of carbonated solutions. The solubility of CO_2 decreases with temperature. We used solubility data from Crovetto to calculate the concentration of CO_2 in water expected at 6 °C following the experimental procedures outlined in Sec. II.[19] The resulting supersaturation in water only at 20 °C was calculated to be $S = 4.3$. The solubility of CO_2 decreases slightly with increasing sucrose concentration; using the data of Vázquez Uña, we calculate $S = 3.9$ at 0.058 mol kg^{-1}, and $S = 3.7$ at 0.47 mol kg^{-1}.[20] The supersaturation decreases by only 6% over this range of sucrose concentrations; this cannot explain the increase in lability shown in Fig. 3.

A possible cause of LIN is pre-existing bubbles. There has been much discussion over whether nanobubbles can exist in bulk solution.[21] Experiments show that some solutes at high concentrations can act to stabilize macroscopic bubbles. Henry and Craig have made measurements of bubble stability over a range of sucrose concentrations.[22] Looking at their data, we see that the degree of stability against bubble coalescence changes by only 3% over the range of sucrose concentrations 0.18–0.47 mol kg^{-1}. These observations concur with data on surface tension, which show <2% increase over the same range of aqueous sucrose concentrations.[23] Such small changes are at variance with the results presented in Fig. 3, which show a 230% increase in lability from $C = 0.18$ to 0.47 mol kg^{-1}. We do not believe that pre-existing nanobubbles are the cause of LIN. By contrast, the approximate factor of 8 increase in lability is close to the factor of 7 increase in concentration from 0.058 to 0.47 mol kg^{-1} for unfiltered sucrose solutions (Table I) and is almost directly proportional to the factor of 7 increase in concentration in this range. This is consistent with the LIN of CO_2 bubbles being due to a population of particles that is proportional to the sucrose concentration.

B. Laser heating of nanoparticles

Absorption of light by nanoparticles has been studied for a range of potential applications, including optical limiting and biomedicine.[24] In particular, a number of groups have studied laser heating of gold nanoparticles, which exhibit high absorption cross-sections due to plasmon resonance; the absorption depends on size and shape of the Au particle.[25] Plech and co-workers have studied vapor bubble formation around Au nanoparticles using time-resolved, optical, and x-ray scattering.[26,27] The results indicate a mechanism involving explosive vaporization of water causing bubble formation. Recent theoretical work suggests that the initial bubble expansion is adiabatic, followed by isothermal collapse.[28,29] During the expansion phase, the nanoparticle becomes isolated thermally from the vapor bubble, which can lead to oscillatory bubble collapse and re-formation, or even melting of the particle.

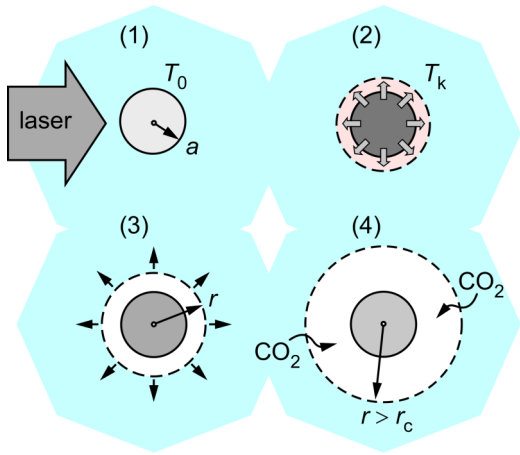

FIG. 5. Mechanistic sequence illustrating the model for producing a water vapor bubble by heating of a nanoparticle. The ambient temperature of the liquid is T_0. In step (1), a nanoparticle (of radius a) absorbs light from the laser pulse, causing it to be heated. In step (2), heat is transferred outwards, raising the temperature of the surrounding liquid; the liquid will vaporize if the liquid temperature goes above the spontaneous boiling temperature (T_k) and will produce an expanding vapor bubble (step 3). In step 4, the bubble will continue to grow if it expands to radius $r > r_c$, where r_c is the critical radius for spontaneous growth of a CO_2 bubble.

In the present work, the results strongly suggest that nanoparticles are responsible for the laser-induced bubble nucleation that we observe, although the composition of the particles is not known. We propose that nucleation occurs due to heating of particles to produce vapor bubbles, and that these bubbles act as seeds for nucleation of CO_2 bubbles. In Fig. 5 we present a schematic diagram to outline the supposed sequence of events.

1. Light is absorbed by the nanoparticle.
2. The absorbed energy is rapidly transferred as heat through the particle to the surrounding liquid.
3. A surrounding shell of liquid is vaporized to produce a bubble.
4. If the resulting bubble reaches a critical threshold radius, it acts as a seed for spontaneous growth by influx of CO_2 from the surrounding fluid.

An accurate model of the nanoscale dynamics of bubble formation and growth due to heating would be very complex, and lies outside of the scope of the present paper. However, we illustrate the feasibility of our mechanism with some simple calculations. In the following discussion, we estimate the radius of a vapor bubble that can be formed in water due to heating of a nanoparticle (Sec. IV C). Then, assuming that such a vapor bubble is formed, we calculate the minimum radius that could support spontaneous growth of a CO_2 bubble (Sec. IV D).

C. Solvent vaporization to produce a bubble

The sequence of steps to produce a vapor bubble is shown in Fig. 5. We assume that the surrounding liquid is pure water (the mole fraction of CO_2 in our solutions is calculated to be 3×10^{-3}), with refractive index $n_w = 1.335$. We assume that the particles are carbonaceous and spherical. The energy absorbed by a spherical particle of radius a can be written as

$$E_{abs} = \pi a^2 Q_{abs}(a)\, u, \tag{2}$$

where Q_{abs} is the absorption efficiency. When the particle is very much smaller than the wavelength of light ($a \ll \lambda$), Q_{abs} can be calculated in the Rayleigh limit.[30] In the present case, $a \sim 100$ nm; therefore, Mie scattering calculations were carried out using MiePlot v4.3 (written by Philip Laven). The complex refractive index of graphite (at 532 nm) is $n_p = 2.691 + 1.456i$.[31] For $a = 100$ nm, we obtain $Q_{abs} = 1.6$. At 14 MW cm^{-2}, the energy density $u = 740$ J m^{-2} and the energy absorbed by the particle $E_{abs} = 3.8 \times 10^{-11}$ J.

We assume that all of the absorbed energy is rapidly transferred to a shell of surrounding water, causing it to be instantaneously heated and vaporized. Values for the spontaneous boiling temperature of water (T_k) reported in the literature vary, depending on the experimental method used, but generally $T_k \sim 0.8T_{cr}$, where $T_{cr} = 647.1$ K is the critical temperature of water.[32,33] The quantity of water that can be heated and vaporized is calculated from the following equation:

$$E_{abs} = n\left(\Delta_{vap}U_{T_1} + \int_{T_0}^{T_1} c_v(T)\mathrm{d}T\right), \tag{3}$$

where n is the number of moles of water, $T_0 = 293$ K, $T_1 = T_k = 520$ K, and c_v is the constant-volume heat capacity of liquid water. At this stage, we assume $\Delta V = 0$; the adiabatic expansion is considered below. The integral in Eq. (3) was calculated using a polynomial fit to heat capacity data obtained from the IAPWS-95 formulation for thermodynamic properties of water.[34] The internal energy change for vaporization was approximated by $\Delta_{vap}U_{T_1} = \Delta_{vap}H_{T_1} - RT_1$, where the enthalpy of vaporization of water $\Delta_{vap}H_{520} = 31$ kJ mol^{-1}.[16] We calculate $n = 9.1 \times 10^{-16}$ mol, corresponding to a volume of water $V_1 = 1.6 \times 10^{-20}$ m^3 at the ambient density $\rho_0 = 998.2$ kg m^{-3}.

The size of the resulting bubble was calculated assuming reversible (isentropic) adiabatic expansion. Assuming an ideal gas, pV^χ = constant, where $\chi = c_p/c_v$ is the ratio of heat capacities; for water at 293 K, $\chi = 1.327$. The initial pressure of the water vapor is estimated to be $p_1 = \frac{nRT_1}{V_1} = 239.6$ MPa. Assuming a final pressure equal to ambient pressure, $p_2 = 100$ kPa, we calculate the final volume of the expanded water, $V_2 = 5.9 \times 10^{-18}$ m^3. Combined with the volume of the particle, this gives a final bubble radius of $r_2 = 1.1$ μm. To compare with the non-ideal case, the specific entropy of the vaporized water $s_1(T_1, \rho_0) = 2.3$ kJ kg^{-1} K^{-1} was calculated from IAPWS-95, which uses the properties of the saturated liquid at the triple point as reference point. The external, ambient pressure was $p_0 = 100$ kPa. Assuming isentropic expansion, the final density of the water $\rho_2(s_1, p_0)$ was calculated to be 3.4 kg m^{-3}, giving the final volume of water $V_2 = 4.8 \times 10^{-18}$ m^3 and a final bubble radius of $r_2 = 1.0$ μm, very close to the ideal case.

The size of bubble produced by nanoparticles of materials other than graphite will depend upon the complex refractive index of the material and on the shape of the particle. For spherical gold nanoparticles with radii $a = 30$ and 100 nm, we estimate $r_2 = 1.4$ and 1.1 μm, respectively; for spherical Fe_2O_3 (hematite) nanoparticles with $a = 30$ and 100 nm, we estimate $r_2 = 0.35$ and 0.78 μm, respectively.

D. Spontaneous growth of carbon dioxide bubbles

The homogeneous nucleation of bubbles from supersaturated solutions of gas has been studied theoretically by Ward *et al.* using a classical thermodynamics approach.[35,36] Excluding effects of water vapor, the critical bubble radius for spontaneous nucleation (r_c) can be written as

$$r_c = \frac{2\gamma}{p_0(S-1)}, \tag{4}$$

where γ is the liquid–gas interfacial tension, p_0 is the external pressure, and S is the supersaturation of gas. From tabulated data for the water–CO_2 system at 100 kPa and 20 °C, we obtain $\gamma = 0.072$ N m^{-1}.[37] Using the value of $S = 4.3$ calculated above, we find $r_c = 0.44$ μm. By including the effects of vapor pressure of the water, this value reduces by only 0.7%. Given the large critical radius, it can be seen that the probability of nucleating a CO_2 bubble spontaneously is exceedingly low. Indeed, all of the nucleation sites observed when opening or pouring carbonated beverages are due to some type of heterogeneous nucleation process.[1,38,39] The vapor bubble radius $r = 1.0$ μm, calculated in Sec. IV C, is larger than the critical radius $r_c = 0.44$ μm. This suggests that laser heating of a nanoparticle could be sufficient to produce a vapor bubble that would continue to grow spontaneously in a supersaturated solution of CO_2.

E. Power threshold and quadratic dependence

The dependence of bubble count on laser power (Fig. 2) was observed to be quadratic. The integer exponent might at first suggest some two-photon excitation process, but this conclusion is not consistent with the femtosecond results. Heating of Au nanoparticles is possible on a sub-picosecond timescale due to the metallic nature of the particles and the strong electron–phonon coupling.[27] The absence of bubbles observed when exposing samples to femtosecond pulses suggests that the heating mechanism is not possible on the short timescale of the pulse; this is likely due to the composition of the particles combined with the comparatively low energy densities.

A possible explanation for the non-linear power dependence is the presence of a distribution of particle sizes in solution. At low laser powers, smaller particles will not produce vapor bubbles that are large enough to cause nucleation of a CO_2 bubble. As the power increases, these smaller particles become active. The non-linear increase in bubble number would occur where there is a larger number of smaller particles. The requirement for a distribution of nanoparticles weighted toward smaller diameters is consistent with measurements of particle size in concentrated solutions, e.g., by optical scattering experiments.[40,41] The nature of the particles, extrinsic or intrinsic, has been the subject of debate.[42,43] Another explanation for the quadratic dependence could be the operation of a secondary nucleation process, whereby at higher powers, multiple vapor bubbles are produced, or a sufficiently large bubble otherwise causes nucleation of more than one CO_2 bubble.

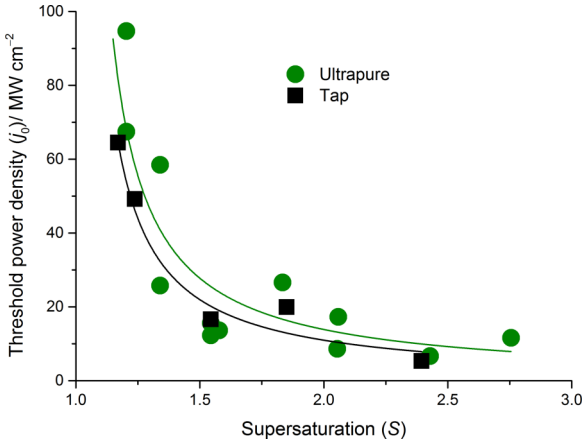

FIG. 6. Graph of threshold laser power density versus supersaturation for LIN of CO_2 from carbonated water. The solid points are the data of Knott *et al.* (at 532 nm) for ultrapure water (circles) and tap water (squares).[10] The solid lines represent fits to the data using the function $j_0 = \alpha(S-1)^{-1}$ (see text for details).

The power threshold can be explained by the requirement for the vapor bubble to expand to at least the critical threshold radius r_c, coupled with the relatively low number of large particles. From our own data, using the non-ideal model in Sec. IV C, we find that the minimum power required to form a bubble of radius $r = r_c = 0.44\ \mu$m is $j_0 = 1.0$ MW cm^{-2}, which is close to the experimentally observed value ~4.8 MW cm^{-2}. Our experiments were conducted at an approximately fixed supersaturation, however. To further validate our model, we have looked at the data of Knott *et al.*, who measured the threshold power density j_0 for aqueous solutions over a range of CO_2 supersaturations, S = 1.2–2.8; their results are reproduced in Fig. 6. If we assume that the threshold power density is proportional to the critical radius, from Eq. (4), we have

$$j_0 = \frac{\alpha}{(S-1)}, \tag{5}$$

where α is a constant parameter. We have fitted the experimental data of Knott *et al.*, see Fig. 8. The quality of the fits is very good; the parameters obtained were $\alpha = 14 \pm 1$ MW cm^{-2} (ultrapure water) and 11 ± 1 MW cm^{-2} (tap water).

F. Implications for NPLIN of crystals

Finally, we discuss the possible connection between LIN of gas bubbles and NPLIN of crystals. Knott *et al.* suggested that bubbles could play a role in NPLIN, even at the low powers where cavitation would not be normally expected. Could NPLIN of crystals be caused by heating of nanoparticles to form vapor bubbles that nucleate the solid phase? A strong piece of evidence is the laser power threshold. We have shown that the magnitude of the threshold for LIN of CO_2 is remarkably similar to that for NPLIN of potassium halide crystals from supersaturated aqueous solutions. Current theoretical models for NPLIN of crystals, such as the optical Kerr effect and the isotropic polarizability model, cannot explain the threshold. By assuming that the vapor bubble must reach a critical radius for nucleation to occur, our model accounts for the laser power threshold.

A significant difference between LIN of the different phases is the power dependence, which appears quadratic for gas and linear for crystals. The explanation for this may lie in the mechanism by which a vapor bubble would cause nucleation of a solid. In order to obtain a quadratic dependence of CO_2 nucleation events with laser power, we suggested the presence of a distribution of nanoparticles with smaller diameters. We consider a dynamical mechanism where the expansion of the bubble causes nucleation of the solid. It is known that ions and solute molecules have different tendencies to adsorb at a gas–liquid interface.[44] The reduced spatial dimensionality of the interface enhances the potential for aggregation. As the bubble expands rapidly, ions or molecules may be swept up and accumulate at the interface leading to nucleation of the solute.

There have been experimental observations of NPLIN of crystals that are difficult to rationalize through the vapor-bubble mechanism. These mostly involve the effect of laser polarization on the product. With urea, Garetz *et al.* noted alignment of the initial crystal of urea along the direction of the electric field of the linearly polarized light.[3] The same group showed that, under certain solution conditions, linearly polarized light forms the γ polymorph of glycine and circularly polarized light forms the α polymorph.[4] The explanation for this could be due to heating of anisotropic nanoparticles, or that the heating process is otherwise polarization dependent.

If LIN is caused by heating of nanoparticles leading to bubbles of vapor, we should wonder why we do not see LIN for all compounds. There are several possible explanations ranging from there being an insufficient concentration of nanoparticles, or that the particles have weak absorption cross-sections, or that the formation of the vapor bubble simply does not promote nucleation of the crystal. We are currently undertaking further experiments, such as intentional doping of solutions, to try to determine the nature of the nanoparticles and to further understand the mechanism for NPLIN of crystals.

V. CONCLUSIONS

In summary, we have carried out a detailed experimental study of LIN of CO_2 gas bubbles. Water and sugar solutions were supersaturated with carbon dioxide gas and exposed to single pulses of laser light of nanosecond or femtosecond duration. It was found that femtosecond pulses did not nucleate bubbles. For the nanosecond pulses, a distinct laser power threshold for nucleation was observed; the magnitude of this threshold was found to be very similar to previous studies of NPLIN of potassium halide crystals from aqueous solution. The number of bubbles produced per laser shot was found to increase with laser power showing a quadratic dependence; this is distinct from the linear dependence on power observed for crystal NPLIN. The number of bubbles produced increases approximately linearly with sucrose concentration and can be reduced dramatically by filtering and cleaning. We have proposed a simple model where nanoparticles are heated by the laser pulse to produce vapor bubbles; to continue growth, these vapor bubbles must attain the critical radius for homogeneous nucleation of CO_2. Our hypothetical model can account both for the laser power threshold for LIN and the quadratic increase in number of bubbles with increasing laser power.

ACKNOWLEDGMENTS

The authors thank Professor Eleanor Campbell and Dr. Olof Johansson for loan of the femtosecond laser system and assistance with the ultrafast experiments. We are grateful to Dr. Philip Camp for useful discussions and to Dr. Brandon Knott and Dr. Baron Peters for sending their nucleation data. We acknowledge the support of the Engineering and Physical Sciences Research Council (EPSRC) (No. EP/G067546/1).

[1]S. F. Jones, G. M. Evans, and K. P. Galvin, Adv. Colloid Interface Sci. **80**(1), 27-50 (1999).
[2]F. Lugli and F. Zerbetto, Phys. Chem. Chem. Phys. **9**(20), 2447-2456 (2007).
[3]B. A. Garetz, J. E. Aber, N. L. Goddard, R. G. Young, and A. S. Myerson, Phys. Rev. Lett. **77**(16), 3475-3476 (1996).
[4]B. A. Garetz, J. Matic, and A. S. Myerson, Phys. Rev. Lett. **89**(17), 175501 (2002).
[5]A. Ikni, B. Clair, P. Scouflaire, S. Veesler, J. M. Gillet, N. El Hassan, F. Dumas, and A. Spasojevic-de Bire, Cryst. Growth Des. **14**(7), 3286-3299 (2014).
[6]A. J. Alexander and P. J. Camp, Cryst. Growth Des. **9**(2), 958-963 (2009).
[7]M. Nardone and V. G. Karpov, Phys. Chem. Chem. Phys. **14**(39), 13601-13611 (2012).
[8]X. Y. Sun, B. A. Garetz, and A. S. Myerson, Cryst. Growth Des. **6**(3), 684-689 (2006).
[9]J. Matic, X. Y. Sun, B. A. Garetz, and A. S. Myerson, Cryst. Growth Des. **5**(4), 1565-1567 (2005).
[10]B. C. Knott, M. F. Doherty, and B. Peters, J. Chem. Phys. **134**(15), 154501 (2011).
[11]B. C. Knott, J. L. LaRue, A. M. Wodtke, M. F. Doherty, and B. Peters, J. Chem. Phys. **134**(17), 171102 (2011).
[12]A. Vogel, N. Linz, S. Freidank, and G. Paltauf, Phys. Rev. Lett. **100**(3), 038102 (2008).
[13]A. Soare, R. Dijkink, M. R. Pascual, C. Sun, P. W. Cains, D. Lohse, A. I. Stankiewicz, and H. J. M. Kramer, Cryst. Growth Des. **11**(6), 2311-2316 (2011).
[14]S. K. Crossno, L. H. Kalbus, and G. E. Kalbus, J. Chem. Educ. **73**(2), 175-176 (1996).
[15]A. H. Harvey, J. S. Gallagher, and J. M. H. L. Sengers, J. Phys. Chem. Ref. Data **27**(4), 761-774 (1998).
[16]*CRC Handbook of Chemistry and Physics*, 86th ed., edited by D. Lide (CRC Press, Boca Raton, FL, 2005).
[17]M. R. Ward and A. J. Alexander, Cryst. Growth Des. **12**(9), 4554-4561 (2012).
[18]J. O. Sindt, A. J. Alexander, and P. J. Camp, J. Phys. Chem. B **118**(31), 9404-9413 (2014).
[19]R. Crovetto, J. Phys. Chem. Ref. Data **20**(3), 575-589 (1991).
[20]G. Vázquez Uña, F. Chenlo Romero, G. Pereira Goncalves, and J. Peaguda Lorenzo, J. Chem. Eng. Data **39**(4), 639-642 (1994).
[21]J. R. T. Seddon, D. Lohse, W. A. Ducker, and V. S. J. Craig, ChemPhysChem **13**(8), 2179-2187 (2012).
[22]C. L. Henry and V. S. J. Craig, Langmuir **25**(19), 11406-11412 (2009).
[23]J. Permprasert and S. Devahastin, J. Food Eng. **70**(2), 219-226 (2005).
[24]*Springer Handbook of Nanomaterials*, edited by R. Vajtai (Springer-Verlag, Heidelberg, 2013).
[25]P. K. Jain, K. S. Lee, I. H. El-Sayed, and M. A. El-Sayed, J. Phys. Chem. B **110**(14), 7238-7248 (2006).
[26]V. Kotaidis, C. Dahmen, G. von Plessen, F. Springer, and A. Plech, J. Chem. Phys. **124**(18), 184702 (2006).
[27]A. Siems, S. A. L. Weber, J. Boneberg, and A. Plech, New J. Phys. **13**, 043018 (2011).
[28]K. Sasikumar and P. Keblinski, J. Chem. Phys. **141**(23), 234508 (2014).
[29]J. Lombard, T. Biben, and S. Merabia, Phys. Rev. Lett. **112**(10), 105701 (2014).
[30]C. F. Bohren and D. R. Huffman, *Absorption and Scattering of Light by Small Particles* (Wiley, New York, 1983).
[31]A. B. Djurišić and E. H. Li, J. Appl. Phys. **85**(10), 7404-7410 (1999).
[32]C. T. Avedisian, J. Phys. Chem. Ref. Data **14**(3), 695-729 (1985).
[33]S. D. Lubetkin, Langmuir **19**(7), 2575-2587 (2003).
[34]W. Wagner and A. Pruß, J. Phys. Chem. Ref. Data **31**(2), 387-535 (2002).
[35]A. S. Tucker and C. A. Ward, J. Appl. Phys. **46**(11), 4801-4808 (1975).
[36]C. A. Ward, A. Balakrishnan, and F. C. Hooper, J. Basic Eng. **92**(4), 695-704 (1970).
[37]B.-S. Chun and G. T. Wilkinson, Ind. Eng. Chem. Res. **34**(12), 4371-4377 (1995).
[38]G. Liger-Belair, G. Polidori, and P. Jeandet, Chem. Soc. Rev. **37**(11), 2490-2511 (2008).
[39]P. M. Wilt, J. Colloid Interface Sci. **112**(2), 530-538 (1986).
[40]L. Li and T. Ogawa, J. Cryst. Growth **211**(1-4), 286-289 (2000).
[41]Y. Georgalis, A. M. Kierzek, and W. Saenger, J. Phys. Chem. B **104**(15), 3405-3406 (2000).
[42]M. R. Ward, S. W. Botchway, A. D. Ward, and A. J. Alexander, Faraday Discuss. **167**, 441-454 (2013).
[43]A. Jawor-Baczynska, J. Sefcik, and B. D. Moore, Cryst. Growth Des. **13**(2), 470-478 (2012).
[44]C. L. Henry and V. S. J. Craig, Langmuir **26**(9), 6478-6483 (2010).